

Oxygen Reduction Studies on Carbon-supported Pt-M Catalysts (M: Ru, W, Mo)

R. Hernández Maya¹, A.J. Armenta González^{1,2,3}, O. Ugalde¹, M.T. Oropeza Guzmán² and P. Roquero^{1,*}

¹Facultad de Química, Universidad Nacional Autónoma de México, Avenida Universidad 3000. México D.F. 04510

²Instituto Tecnológico de Tijuana, Centro de Graduados e Investigación. Baja California, México 22000

³Centro de Investigación y Desarrollo Tecnológico en Electroquímica A.C. Querétaro, México 76703

Received: December 07, 2011, Accepted: February 10, 2012, Available online: March 29, 2012

Abstract: The activities of a series of carbon-supported bimetallic catalysts, with different active phases loadings, were tested towards the oxygen reduction reaction (ORR). Pt was used in all materials and its loading was kept constant. Mo, W and Ru were used as promoting phases. Rotating Disk electrode experiments revealed that Pt-Ru displayed the best performance in oxygen reduction among the studied materials. The materials with the highest loadings of the second metal revealed the highest activities. X-Ray Diffraction studies (XRD) and Transmission Electron Microscopy (TEM) revealed the presence of homogeneously dispersed metallic ruthenium and different tungsten or molybdenum oxides in the corresponding catalysts. No evidence of alloying was found, and thus the catalytic performances appear to be related to the distribution and interaction of the active phases.

Keywords: Oxygen reduction reaction; fuel cell catalyst, platinum, ruthenium, tungsten, molybdenum

1. INTRODUCTION

The oxygen reduction reaction (ORR) is a limiting factor in the development of low-temperature fuel cells, mainly because of the complex reaction mechanisms and the involved slow kinetics [1,2]. Catalysts formulated with platinum supported on carbon have been used in a large number of works, as cathode electrodes because they have proven to be efficient for the four-electron reduction reaction of O₂ to yield water [3,4]. The ORR is a multi-electron reaction that may include a number of elementary steps involving different reaction intermediates. In scheme 1 are presented the different stable intermediates in acidic and alkaline media, and the formal equilibrium potentials associated with each redox couple [5]. Aggressive chemical intermediates can be produced, either in acidic medium (H₂O₂, HOO[•]) or in alkaline electrolytes (O₂^{•-}, HOO^{•-}). The development of catalysts able to provide reaction routes to directly convert O₂ into H₂O or OH⁻ is still a concern for scientists and engineers.

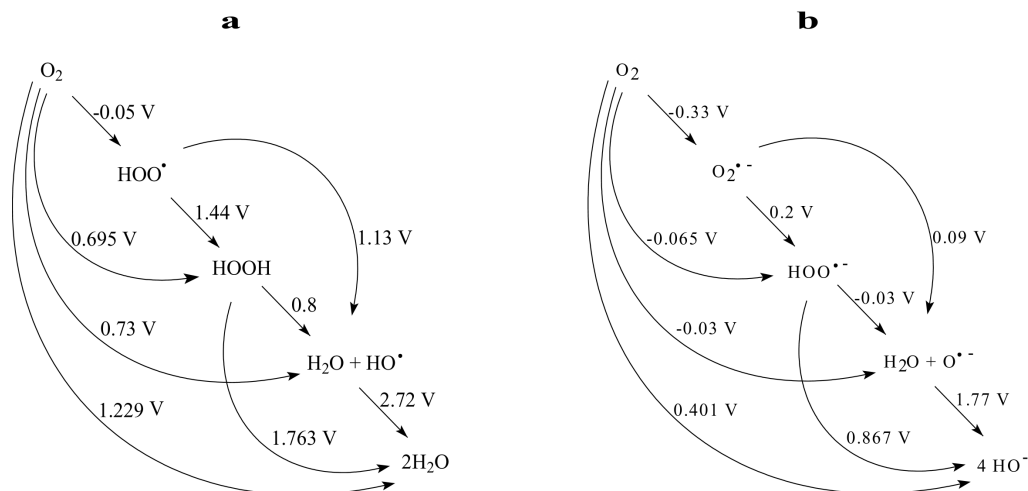
Various reaction pathways for the ORR have been proposed [6,7]. The more widely accepted is illustrated in Scheme 2. Based on this reaction scheme, O₂ can be electrochemically reduced either directly to water with the rate constant k_1 without formation of

adsorbed H₂O₂, or to H₂O_{2ads} with a rate constant k_2 , for the two-electron reduction reaction. The absorbed peroxide can be electrochemically reduced to water with the rate constant k_3 , catalytically decomposed on the electrode surface (k_4) or desorbed to the bulk of the solution (k_5).

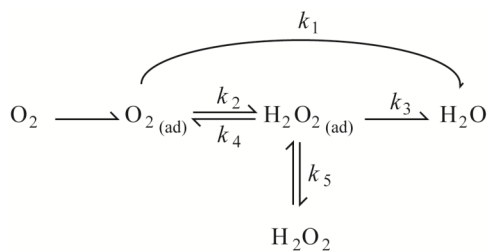
Combination of Pt with other transition elements such as W, Mo, Ru, Sn, [8,9] has revealed good performances of the cathode catalyst layers. The enhanced catalytic activity of bimetallic surfaces in comparison with pure metal surfaces is usually ascribed to two effects: the bifunctional effect in which the unique catalytic properties of each of the elements in the compound is combined and results in a more active surface than each of the elements alone, and the electronic effect in which one of the elements modifies the electronic properties of the other [10,11]. It has been proposed that tungsten promotes hydrogen peroxide reduction [12,13], an intermediate in the complete Oxygen Reduction Reaction (ORR). It has also been reported that Ru-based catalysts exhibit good activity towards the ORR [14,15].

The aim of this work is to evaluate the performance of Ru, W and Mo as promoting phases, in combination with Pt, in cathode catalysts, and to establish the effects related to the proportions of each component.

*To whom correspondence should be addressed: Email: roquero@servidor.unam.mx
Phone:



Scheme 1. Oxygen reduction intermediates and thermodynamic equilibrium potentials referred to the Normal Hydrogen Electrode. a) pH = 0; b) pH = 14



Scheme 2. Reaction mechanisms commonly accepted for O₂ reduction.

2. EXPERIMENTAL PROCEDURE

2.1. Catalysts synthesis and electrode preparation

The synthesis of Pt-M/C catalysts was carried out in a reflux system where Pt carbonyl complex, the second metal (M) carbonyl complex, and vulcan XC72R carbon were dissolved or suspended in *o*-xylene [16].

The temperature was kept at 140 °C and reflux was maintained for 24 h. Once the reaction time was elapsed, the *o*-xylene was distilled, the catalysts were washed with diethyl ether three times and heated at 400 °C in N₂ atmosphere for 1 hour. This synthesis method allows to control Pt particle size during the synthesis of Pt carbonyl compounds. Pt(CO)₆ can easily polymerize with characteristic changes in the dissolution color [17]. The nominal composition of each material is presented in table 1. As it can be seen, the platinum loading was constant in all cases, and the proportions of M and vulcan carbon changed.

A catalytic ink was prepared with 25 mg of the electrocatalyst and 16 mL of a Nafion solution (3% isopropanol). Electrodes were prepared by the deposition of 5 μL of the ink onto the surface of a glassy carbon rotating disk electrode, with a surface area of 0.19 cm². This corresponds to a 2.5 μg catalyst loading in these electrodes. The film was left to dry at room temperature during 12 h

before the tests. In a previous work, the morphology of these layers was investigated by means of Scanning Electron Microscopy, and revealed no important differences in porosity or electrode surface area as a function of the catalyst composition [18].

2.2. Electrochemical experiments

The electrolyte employed in all cases was 0.5 M H₂SO₄ in bidistilled, deionized water. The electrolytes were first degassed by bubbling N₂ for 15 minutes. A Saturated Calomel Electrode (SCE) was employed in all experiments. Results in this work are referred to the Normal Hydrogen Electrode (NHE). The open circuit potential was then measured and cyclic potential sweeps, between -150 mV and 1650 mV vs. NHE were applied in order to activate the working electrode. Afterwards, a potential step was applied at -300 mV vs. SCE in order to clean the surface. The electrolyte is then oxygenated by bubbling O₂ (99.99 %) during 15 minutes.

Preliminary cyclic voltammetry tests were carried out for each catalyst, in order to find redox couples associated with changes in the oxidation states of the elements present in each material.

ORR studies are then carried out in a conventional three-electrode cell, with SCE as reference, a graphite rod as counter electrode and the catalyst on the RDE as working electrode. The experiments consisted of a potential scan from 900 to -160 mV vs. NHE with varying rotation speeds, from 0 rpm to 2000 rpm. Scan rate was kept at 5 mV/s for all experiments.

Table 1. Prepared catalysts, where M designates Ru, W or Mo.

Catalyst designation	Weight percent		
	Pt	M	Carbon
Pt/C	20	0	80
Pt50-M50	20	20	60
Pt67-M33	20	10	70
Pt80-M20	20	5	75
M/C	0	20	80

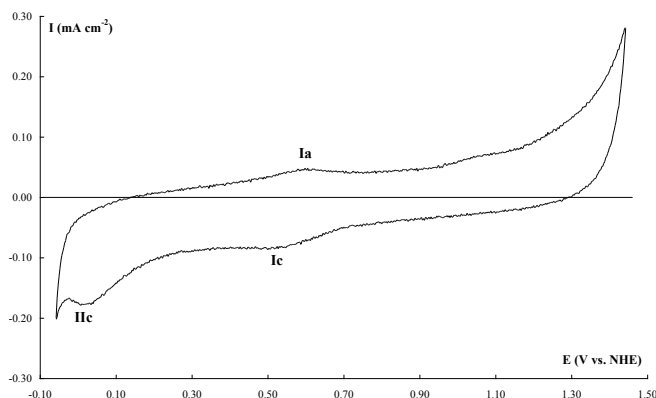


Figure 1. Cyclic Voltammogram from Ru/C, recorded at 100 mV s⁻¹.

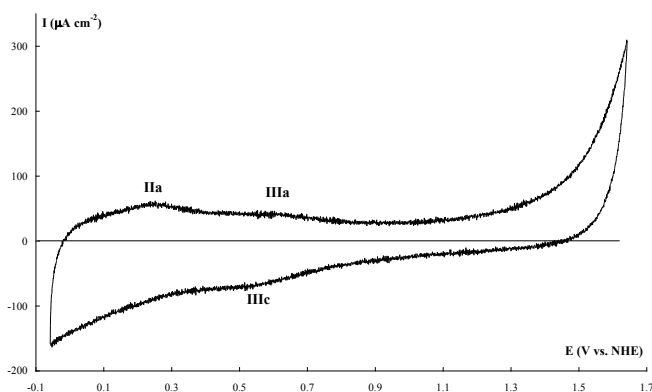


Figure 2. Cyclic Voltammogram from W/C, recorded at 100 mV s⁻¹.

2.3. X-Ray Diffraction measurements

Diffraction patterns were obtained at room temperature using Cu K_α ($\lambda = 1.5406 \text{ \AA}$) radiation on a Siemens D-500 diffractometer, with a speed of 28 min⁻¹.

2.4. Transmission Electron Microscopy

Microscopy samples were obtained from suspensions of each catalyst in n-heptane. A few drops of the supernatant liquid were deposited on 200-mesh copper grids covered with a carbon film. Images were obtained with a JEOL 2010 microscope.

3. RESULTS AND DISCUSSION

Cyclic voltammetry characterizations are presented in figures 1 to 4. The peak labeled Ia in figure 1 is attributed to ruthenium oxidation: Ru(0) to Ru(II) [19]. Another possible oxidation step, though with a very small current, is observed at 1 V vs. NHE. The cathodic peak Ic corresponds to the reversible reduction Ru(II) to Ru(0). The cathodic peak Iic should be related to the proton adsorption preceding hydrogen discharge. Peaks IIa and IIIa in figure 2 are due to tungsten oxidation. In this case only one cathodic peak, IIIc is observed. In figure 3, clear redox behavior of supported molybdenum is shown. Peaks IVa and Va are attributed to Mo(0) to Mo(III) and Mo(III) to Mo(V) oxidations, respectively

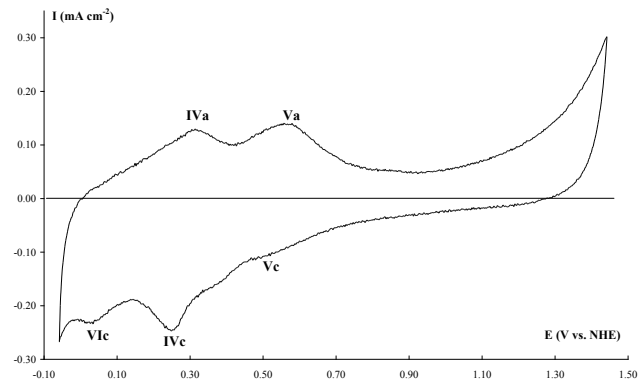


Figure 3. Cyclic Voltammogram from Mo/C, recorded at 100 mV s⁻¹.

[16]. The corresponding reduction steps are also clearly marked and with similar current densities as the forward scan peaks. Peak VIc precedes the hydrogen discharge, as in the case of Ru/C, and could be due to an electron transfer taking place at the carbon support.

In figure 4, the cyclic voltammetry results for Pt-containing materials is presented. Here it is to remark that peak Ia, due to the ruthenium redox behavior, can be clearly seen (figure 4b), as well as peak IVa in the catalyst formulated with molybdenum (figure 4d). The current densities associated with proton-desorption phenomena (in potentials between -0.09 and 0.3 V vs. NHE) are clearly lower in the bimetallic materials than in Pt/C and are considerably suppressed in the W-containing catalyst (figure 4c).

Different polarization curves in RDE experiments, carried out with O₂-degassed and O₂-saturated electrolytes, are presented in figure 5 for the case of the Pt67-Ru33/C catalyst. A shift of 0.11 V in the onset potential between both curves is observed, revealing clearly the applicability of this material as oxygen reduction catalyst. Similar results were obtained with all catalysts, but the larger decrease in the onset potential was the one presented in figure 5.

As an example of the obtained results in rotating disk electrode experiments, in figure 6a is presented the series of polarization curves obtained with Pt67-Ru33, at the studied rotation speeds. Similar curves were obtained with all Pt-containing materials. Here, a diffusion peak can be observed at 0.74 V vs. NHE in the curve without agitation (0 rpm) and it is no longer present in those with forced convection. This is due to the ORR entering the mass transfer control regime. The I-E curves slopes change in this potential domain: the main reduction product is H₂O₂ at potentials between 0.8 and 0.75 V vs. NHE (n=2), and H₂O between 0.75 and 0.6 V vs. NHE (n=4). A diffusion control plateau is then observed in all curves between ~0.55 and 0.2 V vs. NHE. This plateau, however, is not well-defined due most probably to mixed control in this potential domain. Tafel plots, obtained by subtracting the diffusional current [20,21], are presented for the Pt67-M33 series in figure 6b. The highest current is obtained with Pt-Ru and Pt-W materials. The slope change as water becomes the main product is clearly marked for these two catalysts, while for Pt and Pt67-Mo33 the slope change is not observed, the current is considerably lower and H₂O₂ seems to be the predominant product in the whole poten-

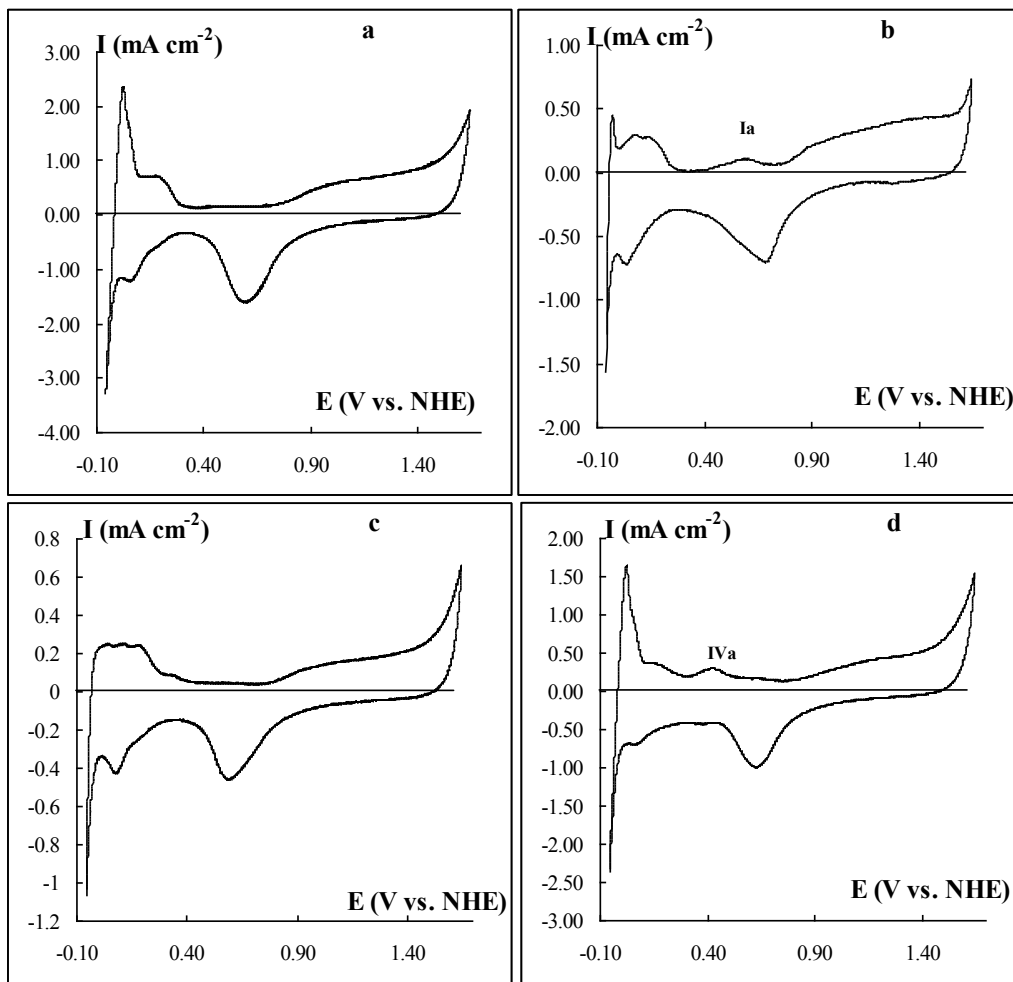


Figure 4. Typical cyclic voltammograms from Pt-containing materials, recorded at 100 mV s^{-1} . a) Pt/C; b) Pt67-Ru33/C; c) Pt67-Mo33/C; d) Pt67-W33/C

tial range. Electron-transfer coefficients, calculated from these slopes in the purely kinetic region are a ~ 0.57 for Pt67-Ru33 and Pt67-W33, and $\alpha \sim 0.51$ for Pt and Pt67-Mo33. At potentials below 0.15 V vs. NHE the cathodic current increases again due to proton chemisorption.

In figure 7, the limiting current is recorded for each set of curves at 0.2 V vs. NHE and plotted against the square root of the rotation speed ($\omega^{1/2}$). A linear dependence of I_L with ω is observed at low rotation speeds. At high ω values, a deviation from this behavior occurs, confirming the mixed control behaviour of the electrical current in this region. It can be seen that Pt50-M50 is, in all cases, the proportion that provides the highest current. Among the three studied promoting phases, ruthenium is the metal that offers the best performances with electrical currents about 2 mA higher than Pt/C.

XRD results, displayed in figure 8, reveal different species formed on the carbon surfaces. Metallic ruthenium is found in Ru/C (figure 8a) and Pt50-Ru50/C (figure 8e) according to JCPDS 01-089-4903. Molybdenum trioxide appears to be the predominant

species in Mo/C (figure 8b) with diffraction lines at $2\theta = 24, 26,$ and 39° (JCPDS 05-0508) and some of its features are also found in the Pt50-Mo50/C catalyst (figure 8g). The material W/C presents diffraction lines that correspond to monoclinic WO_3 (JCPDS 43-1035). However, in the Pt50-W50/C catalyst, the diffraction pattern reveals the presence of orthorhombic WO_2 as the main tungsten species (JCPDS 48-1827). Polycrystalline platinum is found in all catalysts containing this element (figures 8d to g), with diffraction lines at $2\theta = 39, 46, 67, 81$ and 86° , corresponding to the Pt planes (1,1,1), (2,0,0), (3,1,1) and (2,2,2), respectively, (JCPDS 4-0802).

Transmission electron micrographs of monometallic materials and bimetallic catalysts are presented in figures 9 and 10, respectively. Pt particles with average size of 2.5 nm are obtained with uniform dispersion on the support (figure 9a). Ruthenium particles are larger than those of Pt in the monometallic materials (figure 9b) with particle sizes ranging from 3 to 12 nm . Tungsten oxides crystals (figure 9c) are somewhat larger than all other particles and present dimensions around 25 nm length by 8 nm width. Molybdenum particles (figure 9d) present not well defined edges and an

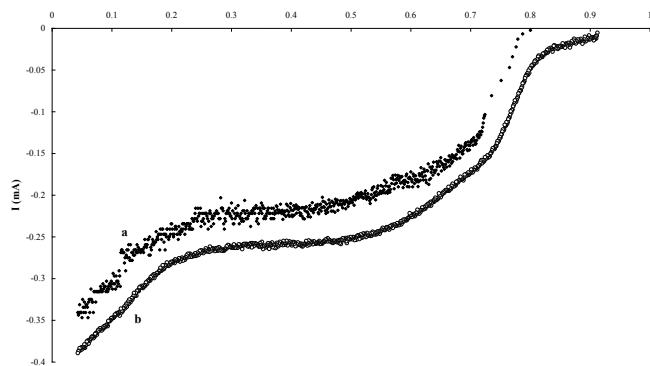


Figure 5. Polarization curves obtained from RDE experiments, at 200 rpm and 5 mV s^{-1} , on Pt67-Ru33/C. a) oxygen purged electrolyte; b) oxygen saturated electrolyte.

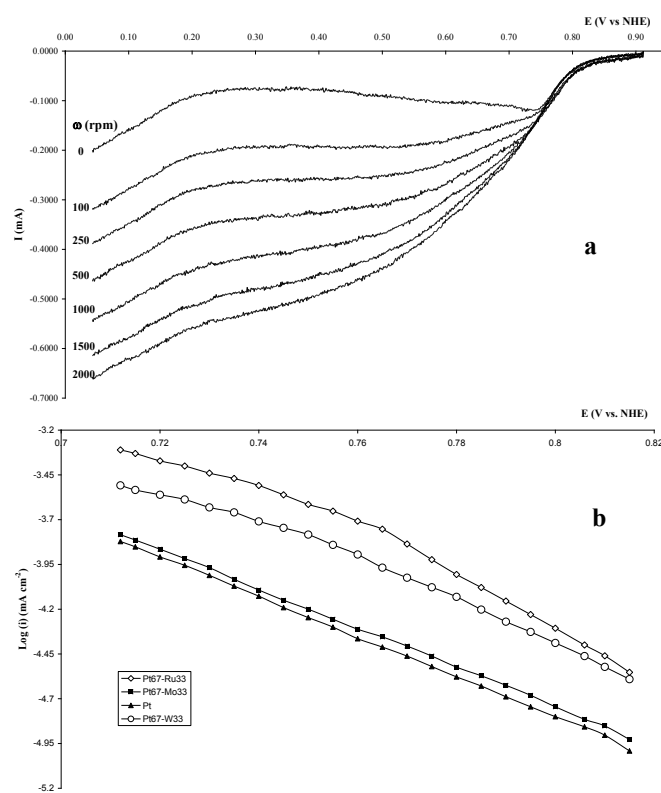


Figure 6. a) Typical polarization curves obtained from Pt67-Ru33 at varying rotation speed, recorded at 5 mV s^{-1} . b) Kinetic current Tafel plots for the Pt67-M33 series.

average particle size of 5 nm.

Images of the bimetallic catalysts, presented in figure 10, show uniform distribution of the Pt crystallites, with the same particle size as the monometallic material, regardless the nature of the second metal phase. In the Pt50-Ru50/C catalyst (figure 10a), both metallic phases appear to be adjacent to each other, and this could be the reason of their enhanced activity. In the Pt50-W50/C material (figure 10b) Pt appears as small particles and tungsten oxide

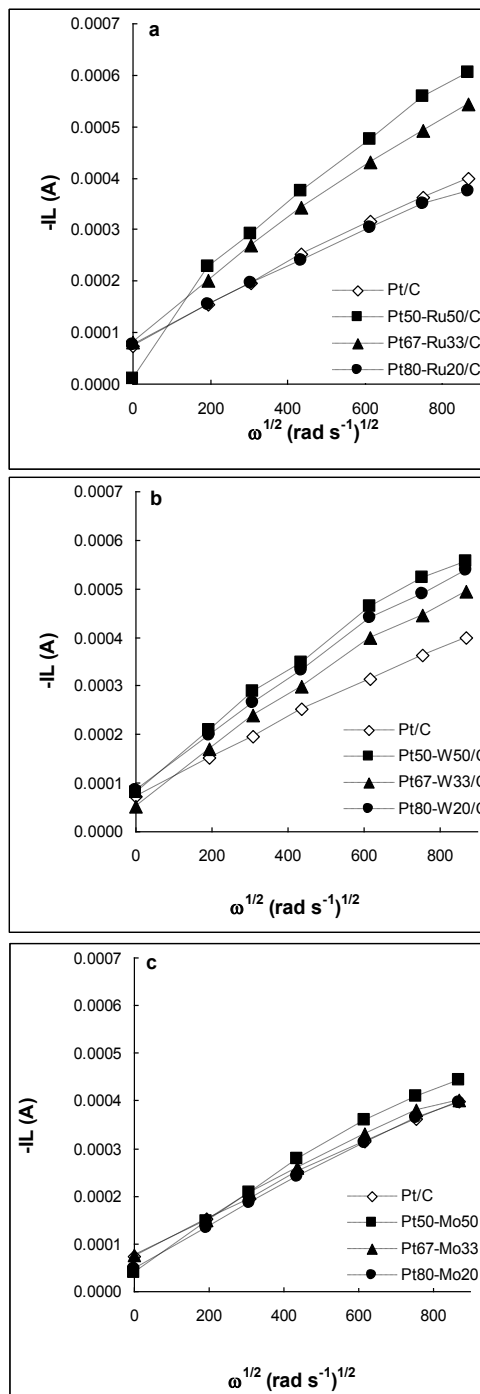


Figure 7. Dependence of the limiting current, recorded at 0.2 V vs. NHE, on the rotation speed ($\omega^{1/2}$) for each catalyst. a) Pt-Ru; b) Pt-W; c) Pt-Mo

crystals can be seen in the center of the image. Pt and W phases are not as close to each other as was the case in Pt-Ru catalysts. In the Pt50-Mo50/C catalyst, it is difficult to identify the Mo oxides, that seem to occupy the same regions as Pt, which presents an increased particle agglomeration.

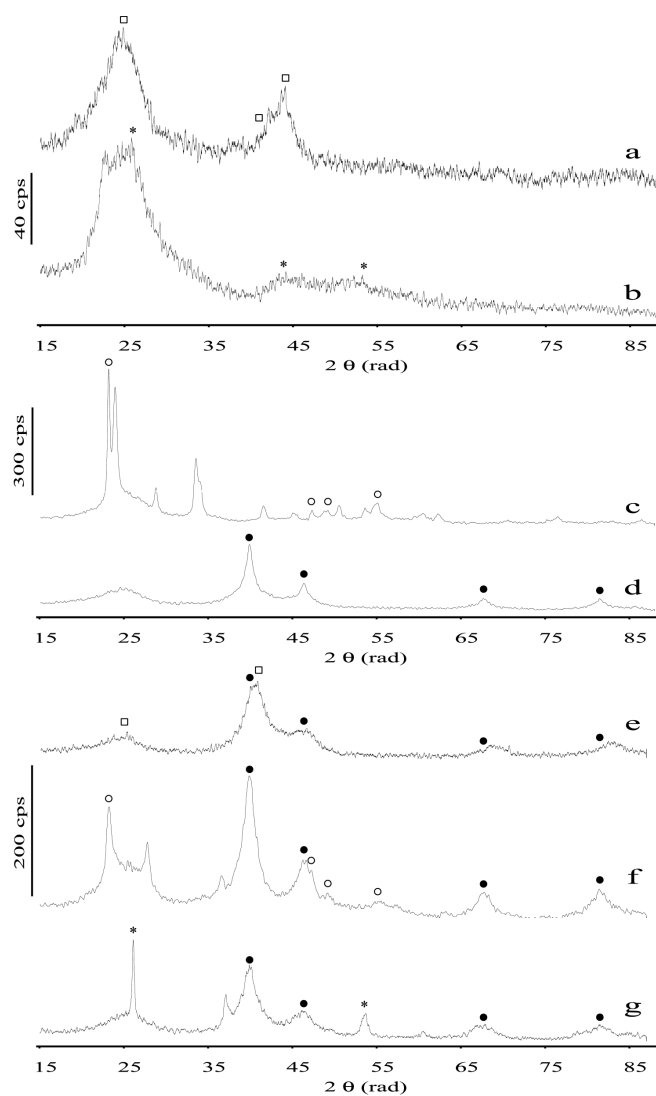


Figure 8. X Ray Diffraction results for the synthesized materials: a) Ru/C; b) Mo/C; c) W/C; d) Pt/C; e) Pt50-Ru50/C; f) Pt50-W50/C; g) Pt50-Mo50/C

4. CONCLUSION

Catalysts with constant Pt loadings and different proportional quantities of a second metal (Ru, W or Mo) and vulcan carbon were synthesized. Ru proved to be the best material to activate, in combination with Pt, the Oxygen Reduction Reaction. Mo yielded poor results when compared with Pt-Ru materials, but still, the electrical currents obtained with Pt50-Mo50 were higher than those observed on Pt alone. High loadings of the second metal improved the catalysts performances, since for all the studied materials Pt50-M50 is the composition that offers the best results. The use of Pt cannot be avoided because none of the M/C materials revealed any oxygen reduction activity.

Employing the same synthesis method, the obtained ruthenium particles are metallic Ru, while tungsten and molybdenum form different oxides. Furthermore, in the W/C material the predominant crystalline species is monoclinic WO_3 , but in the catalysts contain-

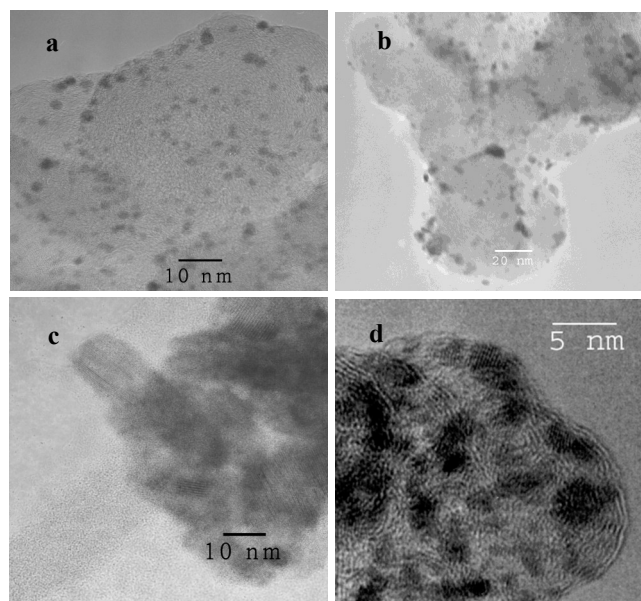


Figure 9. Transmission Electron micrographs of monometallic materials. a)Pt/C;b)Ru/C; c) W/C; d) Mo/C

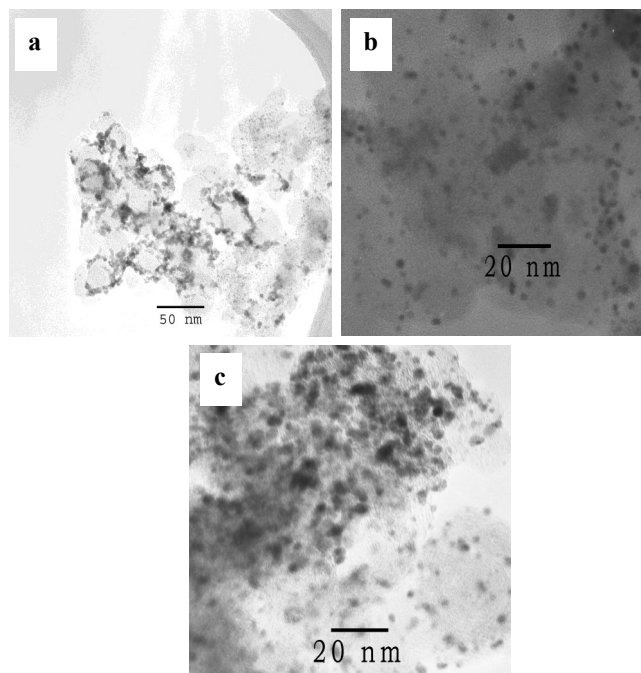


Figure 10. Transmission Electron micrographs of bimetallic catalysts. a)Pt50-Ru50/C ; b) Pt50-W50/C; c) Pt50-Mo50/C

ing platinum and tungsten, orthorhombic WO_2 is the main species. The interaction with Pt during the synthesis procedure, that leads from carbonyl precursors to different oxides, is not yet well understood.

5. ACKNOWLEDGEMENTS

The authors thank Cecilia Saucedo for the obtention of XRD patterns, and Iván Puente Lee for the TEM characterizations. R. Hernández Maya and O. Ugalde acknowledge the scholarships provided by Conacyt, Mexico.

REFERENCES

- [1] G. Liu, H. Zhang, *J. Phys. Chem. C*, 112, 2058 (2008).
- [2] K. Suárez-Alcántara, O. Solorza-Feria, *J. Power Sources*, 192, 165 (2009).
- [3] M. Gustavsson, H. Ekstroem, P. Hanarp, G. Lindbergh, E. Olsson, B. Kasemo, *J. Power Sources*, 163, 671 (2007).
- [4] J.J. Hwang, C.H. Chao, C.L. Chang, W.Y. Ho, D.Y. Wang, *Int. J. Hydrogen Energy*, 32, 405 (2007).
- [5] D.T. Sawyer, *Oxygen Chemistry*, Oxford University Press, 1991.
- [6] B. Wang, *J. Power Sources*, 152, 1 (2005).
- [7] N.M. Marcovic, P.N. Ross Jr, *Surface Science Report*, 45, 117 (2002).
- [8] S. Liao, V. Linkov, L. Petrik. *Appl Catal A: Gen.*, 235, 149 (2002).
- [9] A.S. Arico, P.L. Antonucci, E. Modica, V. Baglio, H. Kim, V. Antonucci, *Electrochim. Acta*, 47, 3723 (2002).
- [10] J.J. Salvador-Pascual, V. Collins-Martínez, A. López-Ortiz, O. Solorza-Feria, *J. Power Sources*, 195, 3374 (2010).
- [11] G. Ramos-Sánchez, H. Yee-Madeira, O. Solorza-Feria, *Int. J. Hydrogen Energy*, 33, 3596 (2008).
- [12] Kulesza P.J., Miecznikowski K., Baranowska B., Skunik M., Fiechter S., Bogdanoff P., *Electrochem Comm.*, 8, 904 (2006).
- [13] D. Meza, U. Morales, P. Roquero, L. Salgado, *Int. J. Hydrogen Energy*, 35, 12111 (2010).
- [14] K. Suárez-Alcántara, O. Solorza-Feria, *Electrochim. Acta*, 53, 4981 (2008).
- [15] R.G. González-Huerta, J.A. Chávez-Carvayar, O. Solorza-Feria, *J. Power Sources*, 153, 11 (2006).
- [16] L.C. Ordóñez, P. Roquero, P.J. Sebastian, J. Ramírez, *Catalysis Today*, 107, 46 (2005).
- [17] J.C. Calabrese, L.F. Dahl, P. Chini, G. Longoni. *J. Am. Chem. Soc.*, 96, 2614 (1974).
- [18] P. Roquero, L.C. Ordóñez, O. Herrera, O. Ugalde, J. Ramírez. *International Journal of Chemical Reactor Engineering*, 5, 1 (2007).
- [19] D.R. Rolison, P.L. Hagans, K.E. Swider, J.W. Long. *Langmuir*, 15, 774 (1999).
- [20] A. Sarapu, K. Tammesvesky, T.T. Tenno, V. Sammelselg, K. Konttri, D.J. Schiffrin. *Electrochem. Commun.*, 3, 446 (2001).
- [21] G. Vásquez-Huerta, G. Ramos-Sánchez, A. Rodríguez-Castellanos, D. Meza-Calderón, R. Antaño-López, O. Solorza-Feria, *Journal of Electroanalytical Chemistry*, 645, 35 (2010).